Broadband and Ultrathin Infrared Stealth Sheets

*Mohammad J. Moghimi, Guangyun Lin, and Hongrui Jiang**

To effectively hide objects and render them invisible to thermographic detectors, their thermal signatures in the infrared (IR) region of the spectrum may be concealed. However, to conceal broadband spontaneous thermal emission of objects, covering the mid- and long-IR is a major obstacle. Here, metallic-dielectric nanostructures and microscale IR emitters are integrated and transferred onto thin flexible substrates to realize IR stealth sheets. The nanostructures absorb and scatter a broad band of IR wavelengths to reduce both reflection and transmission to below 5% across a wide range from 2.5 to 15.5 µm, and thus significantly attenuate the amount of IR signals propagating toward the detectors. Results show that the nanostructures with their unique properties can almost completely conceal the thermal emission from objects and blend them into their surroundings. In addition, micro-emitters thermally isolated from the broadband absorbers can present false thermography to deceive IR detectors and heat-sensing cameras.

The ability to render objects invisible to observers and their detection tools has captivated human imagination throughout history and recently become a rapidly-growing scientific field.[1,2] One fundamental challenge to make objects completely undetectable is to conceal all signatures in the electromagnetic spectrum.[3–5] Invisibility cloaks and microwave (MW) stealth are two prominent approaches to hiding some of the signatures, and have been extensively investigated in recent years.[6–12] The invisibility cloaks bend the background light around objects to conceal them,[13–16] and MW stealth materials reduce the amount of reflected energy from surfaces to minimize the chance of detection.[17,18] However, these techniques only operate at visible (VIS) and MW frequencies, and the functionality is limited to specific wavelengths. In addition to those spectra, thermal signatures of objects in the wide infrared (IR) spectrum must also be hidden to realize IR stealth, which has extremely important defense and law-enforcement applications.[19–21]

The mechanism for IR stealth is substantially different from VIS cloaks and MW stealth owing to the passive nature of IR detection, which only relies on spontaneous emission of objects rather than external illumination.[22] Human bodies and hot parts of vehicles function as wideband IR sources (**Figure 1**a); therefore, heat-sensing cameras can locate them in total darkness and low-visibility conditions (e.g., fog, smoke). The major obstacle to defeat IR detectors is thus to conceal spontaneous emission of objects over a broadband of IR spectrum, most importantly two transmission windows of 3–5 µm and 8–14 µm, within which the IR radiation easily passes through the atmosphere.[23]

So far, various schemes including thermal insulation, metallic reflectors and metamaterial absorbers have been proposed to hide IR radiation and defeat thermal cameras; however, they all face immense challenges such as heat build-up,[24,25] narrow bandwidth and limited hidden areas.[26,27] For instance, metallic walls can block IR radiation but reflections from their surfaces leave thermal signatures in surrounding areas that can be easily detected. Sealed metallic armor and thermal insulation cause heat build-up and increase temperature inside the hidden areas. Furthermore, thermal insulators such as blankets are thick, heavy and cumbersome to use. The superior approach to realizing IR stealth would be to disturb IR propagation toward detectors with advanced composite nanostructures, which allow for the absorption of a wide band of IR radiation with an ultrathin and lightweight sheet.[19,28,29]

Here, we experimentally demonstrate high-performance IR stealth sheets utilizing dielectric nanowires and metallic nanoparticles with unique optical properties, along with a network of air-channels and an array of addressable micro-emitters, as illustrated in Figure 1b. The nanostructures absorb and scatter incident photons to disrupt the wavefront and thus reduce the amount of IR energy propagating toward detectors.[30,31] In terms of material options, silicon with high index of refraction was selected to form dielectric nanowires (Figure 1c) and metallic nanoparticles (Figure 1d) are made of silver with high extinction coefficient.[32] Additionally, arrays of micro-scale emitters are integrated into the sheets to present false thermal signatures for disguise and deception. The stealth sheets are designed to be wideband and can operate in the desired spectra with high efficiency. Moreover, heat does not build up inside the hidden areas but rather dissipates via the nanostructures and cooling air-channels. One promising advantage of this technique is that large sheets can be achieved to hide macroscopic 3D objects, unlike most invisibility cloaks that just hide a small area in 2D space.[33]

Details on the fabrication process are described in the Figure S1, Supporting Information. Silicon nanowires (SiNWs) and silver nanoparticles (AgNPs) are incorporated into a host substrate to achieve dielectric-metallic stealth sheets, as shown in **Figure 2**a

Prof. H. Jiang, Dr. M. J. Moghimi, Dr. G. Lin
Electrical and Computer Engineering Department
University of Wisconsin-Madison
Madison, WI
E-mail: hongrui@engr.wisc.edu

The ORCID identification number(s) for the author(s) of this article can be found under https://doi.org/10.1002/adem.201800038.
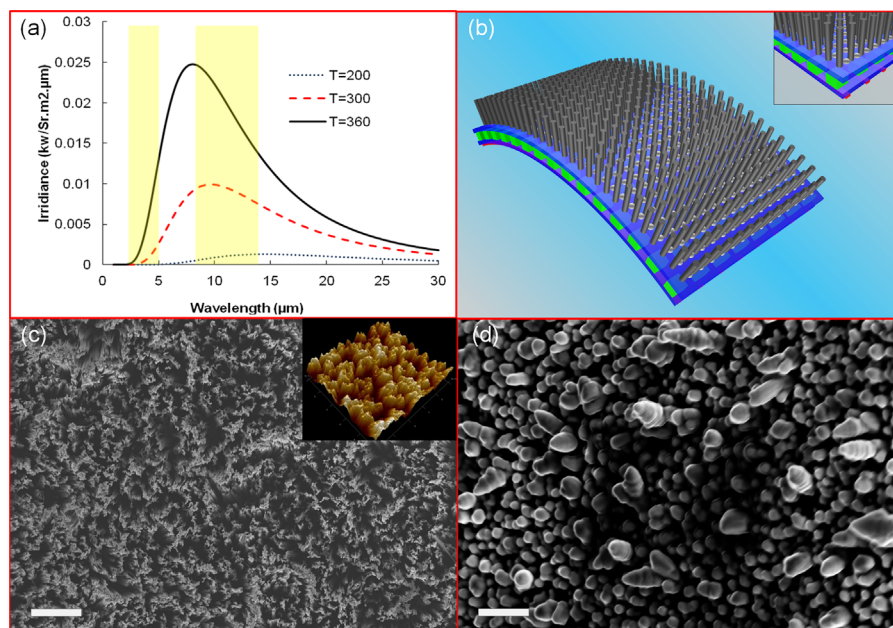
Figure 1. IR emission and stealth sheets with SiNWs and AgNPs. a) Spontaneous emission (black body radiation) and atmospheric transmission windows. The spectral radiation for $T = 360$, 300, and 200 K. The maximum radiation occurs at $\lambda = 8$, 10, and 15 µm, respectively. Straight yellow ribbons show two atmospheric windows 3–5 µm and 8–14 µm, in which IR wavelengths can pass through air and reach to the detectors. b) Schematics of a stealth sheet with nano-scale absorbers, thermal insulation and micro-emitters. The device, implemented on polyimide substrates, is flexible and can be wrapped around objects. Topology of the sheets with nanostructures (gray), air channels between posts (green) and emitters (red). Not drawn to scale. c) SEM of the surface of the SiNWs. The scale bar is 3 µm. Subset: AFM of the SiNW surface to show the morphology of the structures. The total area is 15×15 µm^2. d) SEM of dense AgNPs (viewed from 45°). The scale bar is 200 nm.

and b. The nanostructures are transferred onto a polyimide substrate, which is flexible and can be wrapped around objects. Moreover, the device can have another polyimide layer with addressable micro-emitters to present false IR signature (Figure S2, Supporting Information). The first polyimide layer with embedded nanostructures was bonded to the second polyimide layer with micro-emitters to form the flexible device. Air channels were patterned and formed between these two flexible layers to insulate the absorbers from emitters (Figure S3, Supporting Information). The air channels are open around the edges of the device and form the exhaust for heat dissipation. SiNWs suppress surface reflections and couple maximum fraction of radiation into the nanostructures. The wires (Figure 2a) are partially random in terms of diameters, orientations and density. This randomness allows them to serve as scattering centers and significantly disrupt the wavefront carrying thermographic information, as shown in Figure 2c. In the figure, periodic fluctuations are observed in the electric field distribution along the vertical direction of nanowires because reflections off the nanowires interfere with each other and incident waves. The electromagnetic energy is randomly distributed between SiNWs, as shown in Figure 2c and d. Most energy is confined along SiNWs and the amplitude is enhanced at sharp edges (roughly 5 ×). AgNPs with a high absorption coefficient are distributed between nanowires to decay waves and reduce the transmission to below 5% across the spectrum. Overall, 95% of the electromagnetic energy is absorbed by SiNWs and AgNPs and turned into thermal energy, which is transferred out of the device via the cooling air channels. It is worth noting that warm air is almost invisible to thermal cameras due to extremely low emissivity.

Fourier transform infrared (FTIR) spectroscopy analysis was conducted on the nanostructures and stealth sheet to measure optical characteristics such as reflection, transmission and bandwidth (**Figure 3**). The spectrographs covered a wide range of wavenumbers from 4000 to 650 cm^{-1} ($\lambda = 2.5$ to 15.3 µm), which includes both transmission bands of 3–5 µm and 8–14 µm. To investigate the effect of SiNWs on incident waves, FTIR spectroscopy was performed for a bulk Si wafer before and after etching SiNWs into its surface. Forty eight to fifty five percent of power is reflected from the polished Si surface and 30–35% transmitted through a 380 µm thick Si wafer. In contrast, both reflection and transmission of Si were reduced to below 4% across the spectrum with 11.79 µm-long SiNWs, as depicted in Figure 3a. The reflection from the surface was suppressed by a factor of 20 for the 2.5 µm wavelength and 16 for 15.3 µm. Transmission spectra showed a similar effect with the presence of the nanostructures on Si.

SiNWs serve as an excellent antireflection coating on the device to minimize the reflection from surfaces, and couple the IR energy into the structures.[34,35] Therefore, the dimensions of nanowires are important parameters to determine the performance of the device. SiNWs with a length of 4.64 µm have the maximum reflection and transmission of the studied samples over the whole spectrum. The reflection and transmission are significantly reduced as the length of SiNWs is increased (Figure 3b, c). The wires with 11.79 µm length exhibit the minimal transmission and reflection of the samples in the desired bands. Figure 2d demonstrates the effect of 11.79 µm-long SiNWs with AgNPs on reflection and transmission of
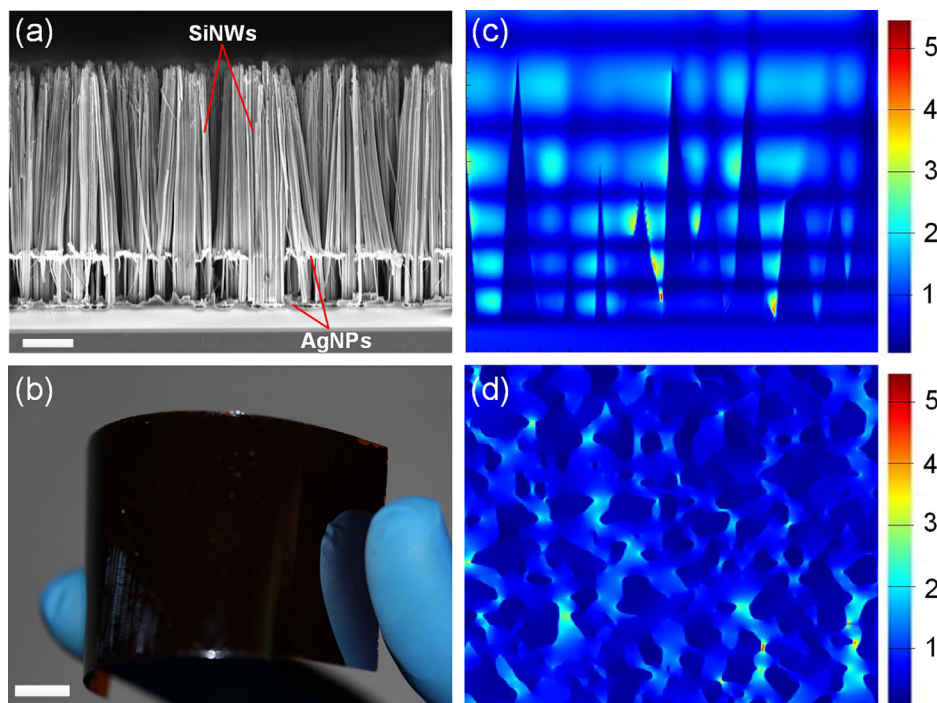
Figure 2. IR stealth sheet with embedded nanostructures. a) SEM of a forest of dense SiNWs 11.79 μm long with diameters varying from 50 to 500 nm. The shape and orientation of wires are partially random. The scale bar is 2 μm. b) Photograph of a completed stealth sheet with a 120 μm thick polyimide layer along with embedded SiNWs and AgNPs. The scale bar is 1 cm. c) FDTD simulation of SiNWs with electric field distribution between wires. The average length of the nanowires is 12 μm and the horizontal length of the simulation area is 4 μm. The wavelength of incident waves is set to 5 μm and its amplitude E_0 is set to 1 v m^{-1} for the simulation. Vertical and horizontal axes are in linear scale. d) Top view of electric field (E) distribution (by FDTD simulation) between wires 6 μm away from the tips of wires (middle of SiNWs). The area of simulation is 4 × 4 μm^2 with linear scale. Color bars represent the amplitude of normalized electric field (E/E_0). The unit for the electric field E is v m^{-1}.

polyimide layers. Polyimide is very transmissive in the desired IR spectra (Figure 3d). However, the presence of nanostructures with a thickness of 11.79 μm drastically reduces the transmission to below 2% and reflection to below 5% within transmission windows of 3–5 μm and 8–14 μm.

As Si is etched deeper and forming SiNWs with a length greater than 12 μm, more energy is trapped and absorbed by the structures, and thus transmission is reduced to below 2% (Figure S5, Supporting Information). However, reflection is slightly increased for nanowires longer than 12 μm. Such high-aspect ratio nanowires tend to break and slightly disturb the index matching capability of SiNWs (Figure S5, Supporting Information). The role of AgNPs in the device is to turn electromagnetic waves into thermal energy because of its high absorption coefficient.[36] The mechanism of absorption here is different from radiative plasmonic resonance in the visible region, which can be excited without SiNWs.[37] The generated heat inside the structures is dissipated with airflows in the channels to the outside of the device.

A forward looking infrared radiometer (FLIR) camera was utilized to detect and image thermal radiation of models representing a human and a vehicle (**Figure 4**a, c), respectively (Supporting Information). We wrapped the models with our flexible stealth sheets (right halves of Figure 4a, c). Two experiments were conducted on the human model and the thermal images were captured with and without a stealth sheet

(Figure 4a). Figure 3b shows the whole model imaged by the IR camera without the stealth sheet (left half). As expected, the model with a temperature of 40 °C can be detected in total darkness with heat-sensing camera. When half covered, the bottom half of the model was detected and imaged while the top half was invisible to the IR camera (right half of Figure 4b). Figure 4c and d shows similar images of a heated model vehicle bare (left) and completely covered by a stealth sheet (right). The vehicle at a temperature of 37 °C was easily detected by the IR camera in darkness; when covered by the stealth sheet it was undetectable, completely blending into its surroundings. The images along with color bars in Figure 4b and d show the temperature profile of the models and their ambient. The background temperature was at 22.5 °C. The thermal images clearly demonstrate the effect of the stealth sheets on IR radiation. Furthermore, the stealth sheet hides objects in low-visibility conditions, where the visual camouflage is not sufficient (Figure S4, Supporting Information). It is worth noting that the stealth sheets did not leave any thermal signature at the surrounding areas owing to the presence of SiNWs with near-zero reflection. In addition, addressable micro-emitters[38,39] can dynamically present false thermal patterns to deceive IR detectors (Figure S6, Supporting Information).

In this study, metallic-dielectric nanostructures composed of AgNPs and SiNWs were utilized to absorb and manipulate spontaneous emission from objects over a broad band in
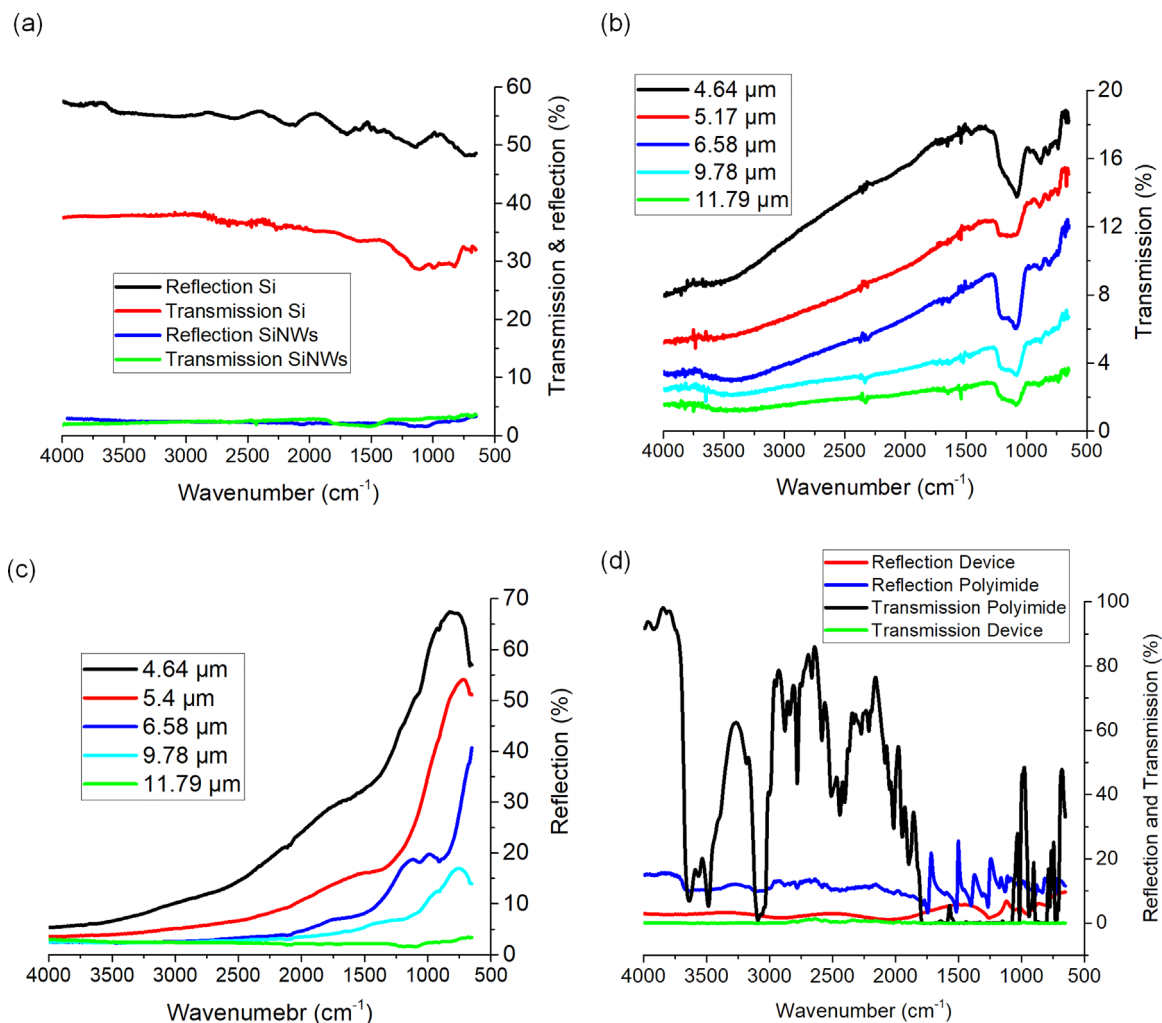
(a)

(b)

(c)

(d)

Figure 3. Measurement results for the spectral range 4000–650 cm^{-1} (2.5 to 15.3 μm). a) Comparison of reflection and transmission of Si with and without SiNWs. Reflection on average is reduced from 50% for bare Si to 3% for SiNWs over the whole spectrum. Transmission on average is reduced from 35% to 3.5% with SiNWs. b) The effect of SiNW length on transmission spectra. Transmission is reduced, and spectral uniformity is improved as the length of SiNWs increases. The minimum transmission occurs with 11.79 μm-long SiNWs. c) The effect of SiNW length on reflection spectra. The maximum reflection occurs with 4.64 μm-long SiNWs with 60% reflection at the wavenumber 1000 cm^{-1} ($\lambda = 10$ μm). This amount is reduced to 3% with SiNWs 11.79 μm long. d) The effect of SiNWs on the flexible polyimide substrate. Most of IR radiation transmits through a polyimide layer 125 μm thick. The average reflection from the polyimide layer is 10%. The reflection and transmission from the final device with 11.79 μm-long SiNWs are drastically reduced to below 5% for the desired spectra.

mid- and long-IR spectra. Our results demonstrate that high-performance IR stealth is feasible, taking advantage of the unique properties of nanostructures with near-zero reflection and transmission. The principle of operation of the stealth sheets mainly relies on suppression of reflection to avoid thermal signatures on the background, and minimize transmitted IR waves reaching the detectors. Toward that goal, our structures significantly manipulate the index of refraction for the IR region of spectrum. Dielectric material (Si) contributes to the real part of the refractive index for index matching and achieve strong anti-reflectance ability. Furthermore, metallic nanoparticles (AgNPs) with a high absorption coefficient significantly increase the imaginary part of the refractive index and decay IR waves.

Integration of addressable micro-emitters can further present deceptive thermography of the object to mislead observers and their detection tools. The micro air-channels between IR absorber and emitters thermally insulate the layers and reduce the interference. In addition, the airflow in the channels ensures that stealth sheets do not heat up and the thermal energy exhausts out of the device in the form of warm air. One of our future work is to install active cooling systems with a feedback control to achieve adaptive stealth sheets for IR wavelengths. The stealth sheets are bendable; however, the limit on the bending radius is determined by mechanical properties of the layers involved and the maximum stress exerted on the device (Figure S7, Supporting Information). The effect of nanowire length was investigated in this work for nanowires with diameters in the range of 250–500 nm. Moreover, the fill factor and the diameter of nanowires influence the absorptivity of the device, which was widely
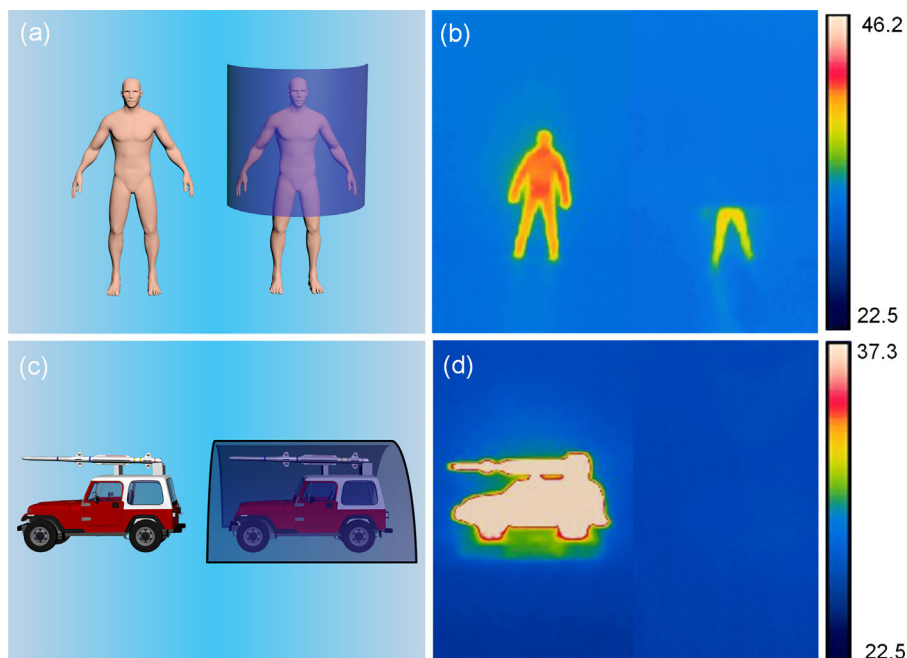
Figure 4. Effect of IR stealth on thermal images. a) A human model with and without the stealth sheet. The top half of the model is covered by a stealth sheet for comparison. b) Thermal images of the human model captured by a FLIR camera. The model without stealth sheet is detectable while the top half of the model covered by the sheet is invisible. c) A vehicle model and the same model completely covered by the stealth sheet. d) Thermal images of the model without stealth (left) and when covered by the stealth sheet (right). Color bars represent temperature (°C).

studied for visible and near IR regions of the spectrum.[31,40] The methods can be extended for IR wavelengths as well. Finally, this IR stealth technique can be combined with VIS camouflage and MW stealth to realize an all-encompassing invisibility method that hides all detectable signatures of objects in the electromagnetic spectrum.

ACKNOWLEDGEMENTS

Supporting Information

Additional supporting information may be found online in the Supporting Information section at the end of the article.

Conflict of Interest

The authors declare no conflict of interest.

Keywords

[1] X. Ni, Z. J. Wong, M. Mrejen, Y. Wang, X. Zhang, *Science* **2015**, *349*, 1310.
[2] C. Yu, Y. Li, X. Zhang, X. Huang, V. Malyarchuk, S. Wang, Y. Shi, L. Gao, Y. Su, Y. Zhang, H. Xu, R. T. Hanlon, Y. Huang, J. A. Rogers, *Proc. Natl. Acad. Sci.* **2014**, *111*, 12998.
[3] U. Leonhardt, T. Tyc, *Science* **2009**, *323*, 110.
[4] S. Xu, H. Xu, H. Gao, Y. Jiang, F. Yu, J. D. Joannopoulos, M. Soljačić, H. Chen, H. Sun, B. Zhang, *Proc. Natl. Acad. Sci.* **2015**, *112*, 7635.
[5] P. Y. Chen, A. Alù, *ACS Nano* **2011**, *5*, 5855.
[6] W. Cai, U. K. Chettiar, A. V. Kildishev, V. M. Shalaev, *Nat. Photonics* **2007**, *1*, 224.
[7] A. Alu, N. Engheta, *Phys. Rev. Lett.* **2008**, *100*, 1.
[8] D. Ye, L. Lu, J. D. Joannopoulos, M. Soljačić, L. Ran, *Proc. Natl. Acad. Sci.* **2016**, *113*, 2568.
[9] J. B. Pendry, *Science* **2006**, *312*, 1780.
[10] P. Hsieh, C. Chung, J. F. McMillan, M. Tsai, M. Lu, N. C. Panoiu, C. W. Wong, *Nat. Phys.* **2015**, *11*, 268.
[11] J. Valentine, J. Li, T. Zentgraf, G. Bartal, X. Zhang, *Nat. Mater.* **2009**, *8*, 568.
[12] N. Landy, D. R. Smith, *Nat. Mater.* **2012**, *12*, 25.
[13] R. Schittny, M. Kadic, T. Buckmann, M. Wegener, *Science* **2014**, *345*, 427.

[14] D. Schurig, J. J. Mock, B. J. Justice, S. A. Cummer, J. B. Pendry, A. F. Starr, D. R. Smith, *Science* **2006**, *314*, 977.

[15] T. Ergin, N. Stenger, P. Brenner, J. B. Pendry, M. Wegener, *Science* **2010**, *328*, 337.

[16] M. Gharghi, C. Gladden, T. Zentgraf, Y. Liu, X. Yin, J. Valentine, X. Zhang, *Nano Lett.* **2011**, *11*, 2825.

[17] L. Deng, M. Han, *Appl. Phys. Lett.* **2007**, *91*, 023119.

[18] O. Balci, E. O. Polat, N. Kakenov, C. Kocabas, *Nat. Commun.* **2015**, *6*, 1.

[19] M. G. Silveirinha, A. Alù, N. Engheta, *Phys. Rev. B* **2008**, *78*, 1.

[20] L. Phan, W. G. Walkup IV, D. D. Ordinario, E. Karshalev, J. Jocson, A. M. Burke, A. A. Gorodetsky, *Adv. Mater.* **2013**, *25*, 5621.

[21] T. Han, X. Bai, J. T. L. Thong, B. Li, C. W. Qiu, *Adv. Mater.* **2014**, *26*, 1731.

[22] M. Pelton, *Nat. Photonics* **2015**, *9*, 427.

[23] Y. Itakura, S. Tsutsumi, T. Takagi, *Infrared Phys.* **1974**, *14*, 17.

[24] N. P. Padture, M. Gell 1, E. H. Jordan, *Science* **2002**, *296*, 280.

[25] M. Hellwig, *Camouflage net, 5348789,* US Patent, C. F. Ploucquet GmbH & Co., Öhringen, Federal Republic of Germany **1994**.

[26] J. Kim, K. Han, J. W. Hahn, *Sci. Rep.* **2017**, *7*, 1.

[27] L. Cai, A. Y. Song, P. Wu, P. Hsu, Y. Peng, J. Chen, C. Liu, P. B. Catrysse, Y. Liu, A. Yang, C. Zhou, C. Zhou, S. Fan, Y. Cui, *Nat. Commun.* **2017**, *8*, 1.

[28] M. A. Kats, R. Blanchard, S. Zhang, P. Genevet, C. Ko, S. Ramanathan, F. Capasso, *Phys. Rev. X* **2014**, *3*, 1.

[29] X. S. Tang, *Carbon nanotube coatings for visible and IR camouflage, 0137324A*, US Patent, Waterloo, CA **2013**.

[30] J. Zhu, Z. Yu, G. F. Burkhard, C. Hsu, S. T. Connor, Y. Xu, Q. Wang, M. McGehee, S. Fan, Y. Cui, *Nano Lett.* **2009**, *9*, 279.

[31] G. Broenstrup, N. Jahr, C. Leiterer, A. Csaki, W. Fritzsche, S. Christiansen, *ACS Nano* **2010**, *4*, 7113.

[32] A. J. Moses, *Refractive Index of Optical Materials in the Infrared Region*, Hughes Aircraft Co., Culver City, CA, DS166 **1970**.

[33] L. H. Gabrielli, J. Cardenas, C. B. Poitras, M. Lipson, *Nat. Photonics* **2009**, *3*, 461.

[34] Y. Nishijima, R. Komatsu, S. Ota, G. Seniutinas, A. Balčytis, S. Juodkazis, *APL Photonics* **2016**, *1*, 076104.

[35] P. Spinelli, M. A. Verschuuren, A. Polman, *Nat. Commun.* **2012**, *3*, 692.

[36] S. Y. Kang, I. C. Jeon, K. Kim, *Appl. Spectrosc.* **1998**, *52*, 278.

[37] D. V. Guzatov, S. V. Vaschenko, V. V. Stankevich, A. Y. Lunevich, Y. F. Glukhov, S. V. Gaponenko, *J. Phys. Chem. C* **2012**, *116*, 10723.

[38] A. Tadaka, *Infrared Phys.* **1983**, *23*, 187.

[39] P. T. Bryant, J. Oleson, S. W. McHugh, E. Beuville, J. D. Schlesselmann, J. T. Woolaway, S. Barskey, S. L. Solomon, T. W. Joyner, in *SPIE Technologies for Synthetic Environments: Hardware-in-the-Loop Testing VII, 4717*, SPIE, Orlando, Florida **2002**.

[40] O. H. AL Zoubi, T. M. Said, M. A. Alher, S. EL Ghazaly, H. Naseem, *Opt. Express* **2015**, *23*, A767.